Geophysical Research Letters

RESEARCH LETTER
10.1029/2024GL109129

Key Points:

- Deep weathering may be due to enhanced permeability and surface area from inherited rock damage from local geologic and tectonic conditions
- Weathering and water flow extend to the elevation of the adjacent first-order intermittent stream channel
- The deep weathering and fracturing front may allow for inter-basin water flow in headwater catchments

Supporting Information:

Supporting Information may be found in the online version of this article.

Correspondence to:

R. P. Callahan,
russell.callahan@uconn.edu

Citation:

Callahan, R. P., Huang, M.-H., Donaldson, A., Hudson-Rasmussen, B., & Zimmer, M. (2024). Geologic and tectonic controls on deep fracturing, weathering, and water flow in the central California Coast Range. *Geophysical Research Letters*, *51*, e2024GL109129. https://doi.org/10.1029/2024GL109129

Received 11 MAR 2024
Accepted 2 JUN 2024

Author Contributions:

Conceptualization: Russell P. Callahan, Mong-Han Huang, Margaret Zimmer
Data curation: Russell P. Callahan
Formal analysis: Russell P. Callahan, Amanda Donaldson, Berit Hudson-Rasmussen
Funding acquisition: Margaret Zimmer
Investigation: Russell P. Callahan, Mong-Han Huang, Amanda Donaldson, Berit Hudson-Rasmussen, Margaret Zimmer
Methodology: Russell P. Callahan, Mong-Han Huang, Amanda Donaldson, Berit Hudson-Rasmussen, Margaret Zimmer
Project administration: Margaret Zimmer
Supervision: Margaret Zimmer

Geologic and Tectonic Controls on Deep Fracturing, Weathering, and Water Flow in the Central California Coast Range

Russell P. Callahan[1,2], Mong-Han Huang[3], Amanda Donaldson[1], Berit Hudson-Rasmussen[3], and Margaret Zimmer[1]

[1]Department of Earth and Planetary Sciences, University of California, Santa Cruz, CA, USA, [2]Department of Earth Sciences, University of Connecticut, Storrs, CT, USA, [3]Department of Geology, University of Maryland, College Park, MD, USA

Abstract The creation of fractures in bedrock dictates water movement through the critical zone, controlling weathering, vadose zone water storage, and groundwater recharge. However, quantifying connections between fracturing, water flow, and chemical weathering remains challenging because of limited access to the deep critical zone. Here we overcome this challenge by coupling measurements from borehole drilling, groundwater monitoring, and seismic refraction surveys in the central California Coast Range. Our results show that the subsurface is highly fractured, which may be driven by the regional geologic and tectonic setting. The pervasively fractured rock facilitates infiltration of meteoric water down to a water table that aligns with oxidation in exhumed rock cores and is coincident with the adjacent intermittent first-order stream channel. This work highlights the need to incorporate deep water flow and weathering due to pervasive fracturing into models of catchment water balances and critical zone weathering, especially in tectonically active landscapes.

Plain Language Summary The creation of fractures in bedrock facilitates water movement through the subsurface which breaks down rock creating porous soil and weathered bedrock. Water movement is vital for important processes like plant growth, streamflow, and groundwater recharge. However, understanding how fracturing, water flow, and rock weathering interact is challenging because the subsurface is difficult and expensive to measure. Here we use observations from drilling, water level monitoring, and geophysics to understand these interactions. Our results indicate that the subsurface is highly fractured due to the geologic and tectonic setting. The large number of fractures makes it easier for water to flow through the subsurface and causes chemical alteration of bedrock. This may cause water to flow outside of the catchment through the subsurface. This work highlights the role of geologic and tectonic processes in driving fracturing, which dictates the movement of water and subsurface weathering beneath Earth's surface.

1. Introduction

Deep weathering below Earth's surface opens pores and fractures in bedrock, altering permeability and influencing how water moves through and is stored within hillslopes. Pore space created by weathering increases the capacity of the subsurface to store water (Rempe & Dietrich, 2018), which is used by vegetation during droughts (Callahan et al., 2022; McCormick et al., 2021). Water moving through deep flowpaths in hillslopes also contributes baseflow to streams, providing refugia for aquatic organisms during dry periods (Dralle et al., 2023). Given the importance of deep weathering to a broad range of processes, incorporating the structure of weathered rock into conceptualizations and models of hydrology and Earth system processes is vital to understanding how water and forest resources will respond to climate change (Fan et al., 2019). However, because weathering is controlled by multiple and often complex processes (Riebe et al., 2017), quantifying the structure and properties of weathered material across landscapes is challenging.

Subsurface water flow exerts a strong control on the depth and degree of subsurface weathering (e.g., Lebedeva & Brantley, 2013). Additionally, the water table elevation may control the initiation of weathering at the base of the critical zone (e.g., Rempe & Dietrich, 2014; Ruxton & Berry, 1959). Conversely, the depth to unweathered bedrock is commonly assumed to impose a no-flow boundary (Freeze & Cherry, 1979) that directs water laterally through the subsurface. In steep headwater systems it is often assumed that subsurface flow paths mirror topography (Hubbert, 1940; Toth, 1963) directing flow to the channel and limiting interbasin transfer of water.

Visualization: Russell P. Callahan, Mong-Han Huang
Writing – original draft: Russell P. Callahan
Writing – review & editing: Russell P. Callahan, Mong-Han Huang, Amanda Donaldson, Berit Hudson-Rasmussen, Margaret Zimmer

These assumptions form the basis for catchment water balances which are routinely used in hydrologic studies. However, in landscapes with deep weathering and high permeability these assumptions may not be valid and water may exit catchments through the subsurface (e.g., Gleeson & Manning, 2008).

Many models of subsurface water flow and weathering do not account for preexisting fractures in the subsurface which enhance permeability and provide surface area for weathering (Andrews & Navarre-Sitchler, 2021). However, many field studies have documented the importance of fractures to chemical weathering (Krone et al., 2021), groundwater recharge (Uchida et al., 2003), streamflow (Payn et al., 2012), and solute generation (McIntosh et al., 2017). Fracturing can arise due to a variety of processes including exhumation (e.g., DiBiase et al., 2018; Molnar et al., 2007), tectonic and topographic stresses (e.g., St Clair et al., 2015), and active tectonics (e.g., Brooks et al., 2017; Savage & Brodsky, 2011) that happen deep beneath the surface and thus remain hard to quantify. Furthermore, understanding connections between weathering, fracturing, and water movement through the critical zone remains a challenge due to a lack of paired measurements of hydrology and subsurface weathering. Here we overcome these challenges by using borehole drilling, geophysical measurements, and hydrologic monitoring to quantify subsurface stucture and water table dynamics to explore connections between water flow, fracturing, and chemical weathering in the deep critical zone.

2. Materials and Methods

2.1. Study Site and Description

Arbor Creek Experimental Catchment herein referred to as Arbor Creek (0.04 km^2) lies within Blue Oak Ranch Reserve located in the Diablo Mountain Range in central coastal California (Figure 1). Arbor Creek has a Mediterranean climate with cool, wet winters and warm, dry summers. The average annual rainfall from 2012 to 2021 was 600 mm and average temperature was 14°C (A. M. Donaldson et al., 2023). Vegetation at the site varies by aspect, with north to northeast facing slopes characterized by oak woodlands and south to southwest facing slopes characterized by seasonal grasses (A. Donaldson et al., 2024). The geology in the region around Arbor Creek is broadly characterized as the Franciscan Complex, which formed in the subduction zone off the west coast of North America (Dibblee & Minch, 2005). Observations from outcrops and drill cores at the site suggest that the bedrock within Arbor Creek is predominantly composed of metagraywacke with some sections of interbedded shale (KJsed; Figure 1). Adjacent to Arbor Creek is a unit of heterogeneous metamorphosed sedimentary rock, where blueschist and other metamorphic minerals are present (KJmet; Figure 1). The site is located 2 km northeast from the Calaveras fault, a right-lateral strike-slip fault that is part of the larger San Andreas fault system (Figure 1a). Major earthquakes have occurred along the fault as recently as October 2022, when the M5.1 Alum Rock Earthquake occurred just 11 km from Arbor Creek (USGS, 2022).

2.2. Borehole Drilling and Core Characterization

In November 2021 we conducted a drilling campaign to directly characterize subsurface weathering, verify geophysical survey results, collect core samples, and monitor hydrologic dynamics in the resulting boreholes. We used augering, split-spoon sampling, and diamond-core water rotary techniques to drill 12 boreholes. Here we focus on the two deepest boreholes, N4W1 and S3W1, where core was retrieved using water rotary drilling. N4W1 is located on the ridge above the north-facing slope and was drilled to a depth of 40.8 m and S3W1 is located on the ridge above the south-facing slope and was drilled to a depth of 27.7 m (Figure 1b). We also utilized a portable gas powered drill to install an in-stream well (StW1) to monitor hydrological dynamics beneath the stream channel. Following the drilling campaign, we dried core at ambient room temperature conditions, removed stains by wiping each core with a wet rag and then photographed and further characterized each core box.

2.3. Seismic Refraction

To characterize how subsurface weathering varies across Arbor Creek we quantified variations in primary-wave velocity (V_P) using active-source seismic refraction surveys. Seismic survey locations were selected to span variations in topographic position to quantify spatial variations in subsurface weathering (Figure 1b). Seismic surveys were conducted between August 2021 and May 2022 using 48 14-Hz vertical component geophones and a Geode recording system. The V_P first-arrival times for each shot-geophone pair were picked using *Pickwin* (Geometrics, Inc.) and inverted for V_P using a THB rj-MCMC inversion scheme developed by Huang

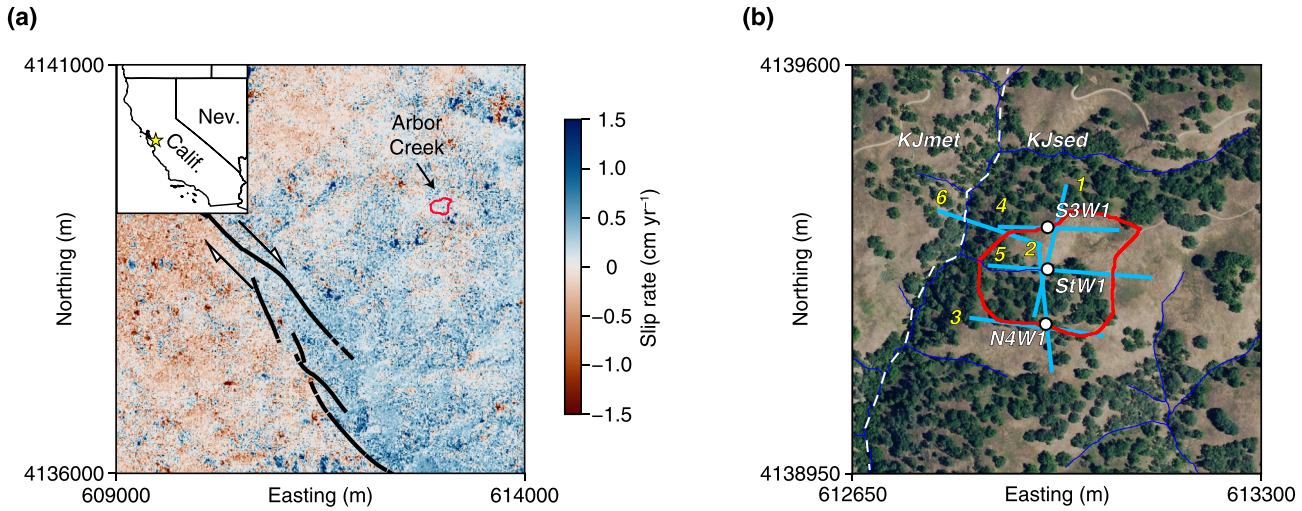

Figure 1. Calaveras fault and Arbor Creek. (a) Inset map of California showing location of study site (star). Main map shows estimates of rates of ground motion in cm yr^{-1} along the Calaveras fault (Charles & William, 2010) (black lines) from a Synthetic Aperture Radar interferogram (Text S2 in Supporting Information S1). The direction of ground movement is indicated by arrows along the fault boundary. Positive values (cool colors) indicate southeast and/or uplift movement and negative values (warm colors) indicate northwest and/or subsident movement. The Arbor Creek catchment (red outline) is less than 2 km from the main fault. (b) Locations of geophysical surveys (blue lines) and boreholes (white circles) within Arbor Creek (red outline). Line numbers are located at the starting point of each geophysical survey. The approximate geologic contact (white dashed line) shows boundary between sedimentary greywacke (KJsed) and mélange rocks (KJmet) with greater metamorphism.

et al. (2021). For details on the survey geometry and inversions for each line see Text S1 and Table S1 in Supporting Information S1.

2.4. Monitoring Deep Groundwater Levels

We measured groundwater levels in N4W1, S3W1, and StW1 every 10 min using pressure transducers placed on kevlar cords just above the bottom of the borehole. A barometer located ~50 m away from S3W1 was used to correct the water level data for variations in atmospheric pressure.

3. Results

3.1. Variations in Weathering From Drilling

Based on borehole drilling and previous soil pit excavations we can broadly divide the subsurface into five different layers (Figure 2). The layers include physically mobile soil, saprolite, weathered bedrock with matrix oxidation, weathered bedrock with fracture oxidation, and fractured bedrock with no oxidation. The depth of mobile soil varies from 0.3 to 0.8 m (A. M. Donaldson et al., 2023). Defining the depth of saprolite is challenging because the boundary between saprolite and weathered rock is difficult to sample and can be gradual, particularly in sedimentary rocks (Hudson Rasmussen et al., 2023). Previous studies have defined the depth of saprolite based on when the rock is competent enough to not collapse during drilling (Callahan et al., 2020; Flinchum et al., 2018) (i.e., the depth when drillers switch from augering to coring). Using this definition, the depth of saprolite is 3.1 m below the surface at N4W1 and 5.2 m below the surface at S3W1. We identified the depth to the other weathering layers by visually observing the cores for red and orange coloring indicative of oxidation of Fe-bearing minerals. The deepest extent of matrix oxidation is 20.4 m below the surface at N4W1 and 17.4 m below the surface at S3W1. Below these depths, oxidation is minimal in the rock matrix, but fractures are oxidized. Oxidation along fracture planes extended to 36.6 m below the surface at N4W1 and 24.7 m below the surface at S3W1. Below these depths there are no visual signs of chemical alteration. However, the cores still have abundant fractures through the bottom of the boreholes, which are 40.8 and 27.4 m below the surface for N4W1 and S3W1, respectively (Figure 2 and Figures S1 and S2 in Supporting Information S1).

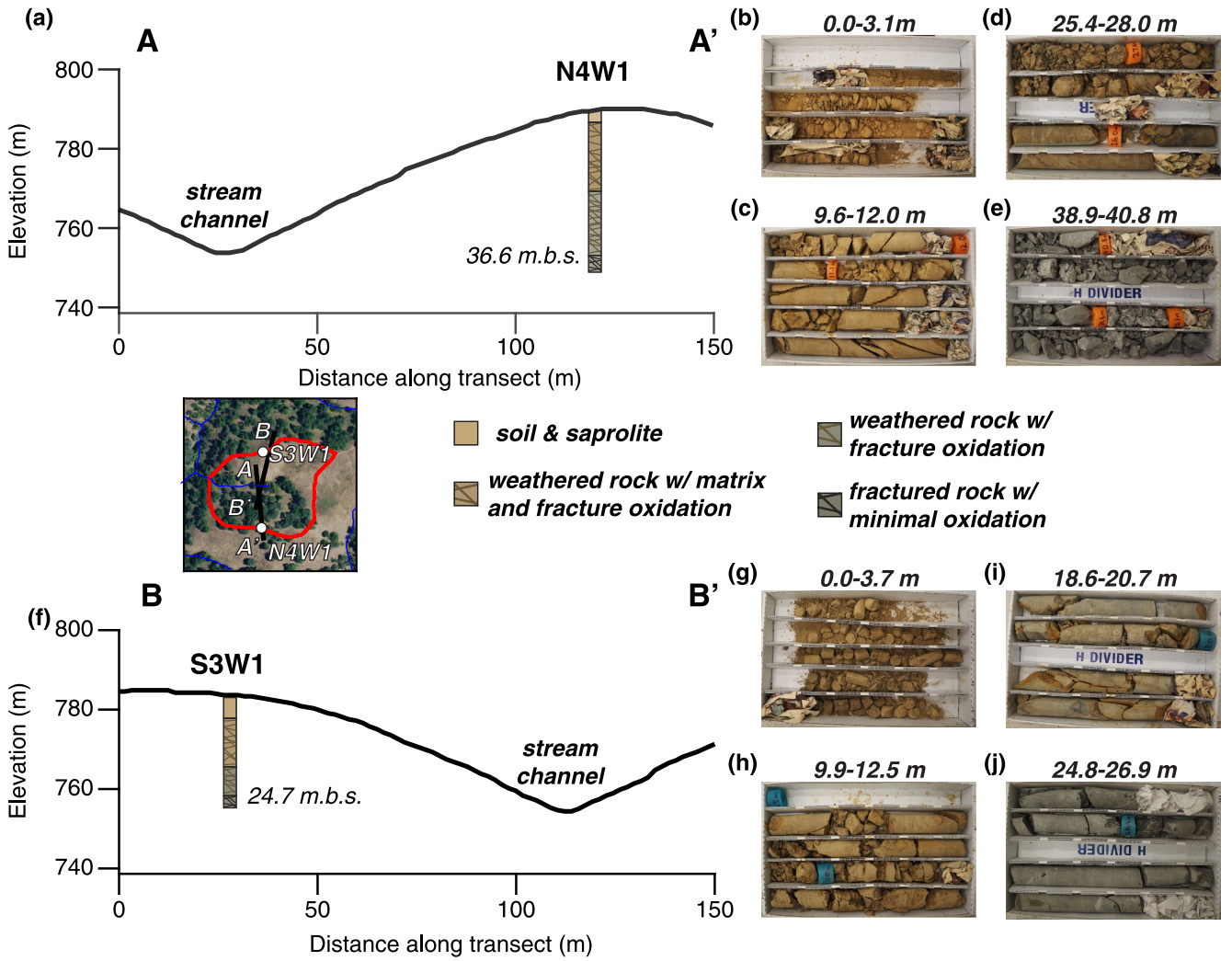

Figure 2. Observations of critical zone structure from borehole drilling. Topographic cross sections (black line) along transects (inset map) with observations from borehole drilling at N4W1 (a) and S3W1 (f). Oxidation along fracture planes was observed 36.6 and 24.7 m below the surface (m.b.s.) at N4W1 and S3W1, respectively. Subsurface structure at Arbor Creek can broadly be divided into soil and saprolite (b and g), weathered rock with matrix and fracture oxidation (c and h), weathered rock with fracture oxidation (d and i), and fractured rock with minimal oxidation (e and j).

3.2. Spatial Variations in Weathering Inferred From Seismic Refraction

To quantify spatial variations in weathering we identified the mean seismic velocities from the surveys at the borehole locations to determine the velocity at the weathering interfaces (Figure S3 in Supporting Information S1). The velocity at the interface between saprolite and weathered bedrock was 1.1 ± 0.3 km s^{-1} (mean ± s.e.m.) and the velocity at the interface between fractured rock with oxidation and unoxidized fractured rock was 2.4 ± 0.3 km s^{-1}. This is consistent with previous work in weathered sedimentary rocks in California which identified velocities of 1.3 ± 0.2 km s^{-1} at the saprolite-weathered bedrock interface and 2.0 ± 0.4 km s^{-1} at the interface between fractured rock with oxidation and unoxidized fractured rock (Hudson Rasmussen et al., 2023). The velocity at the deeper interface is on the low end of lab measurements of unweathered sandstones (2.4–5.6 km s^{-1}) (Mavko et al., 2009). This is likely due to substantial bedrock fracturing at our site.

The depth to the saprolite and weathered bedrock interface (V_P = 1.1 km s^{-1}) ranges from 0 to 8 m across the landscape and is generally thicker at ridge tops and thinner in the valley bottoms of Arbor Creek (e.g., Lines 1 and 2; Figure 3). Additionally, we observed a very thin zone of saprolite along the channel of Arbor Creek (Line 5). Lines 3 and 4 along the ridge tops show variations in the depth to 1.1 km s^{-1}, but do not show systematic patterns.

10.1029/2024GL109129

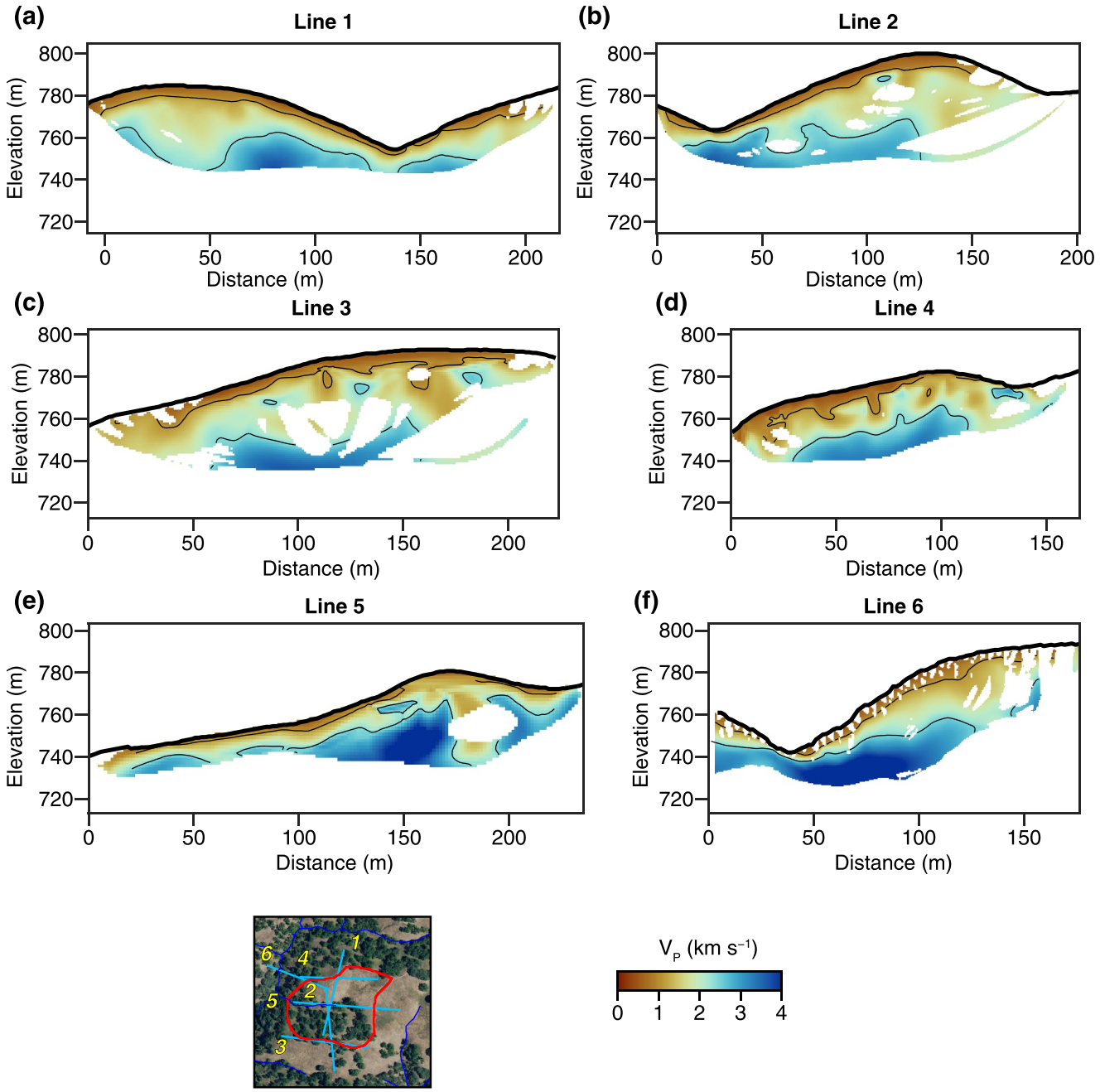

Figure 3. Weathering depths inferred from seismic refraction surveys. (a–f) Cross-sections of mean V_P inferred from seismic refraction surveys. The colorbar represents the mean V_P from all model runs (Text S1 in Supporting Information S1). The surface topography is shown as the solid black line. White areas below the topography represent areas without ray coverage or areas with large uncertainty. Uncertainty and velocity gradient for each survey are shown in Figures S4–S9 in Supporting Information S1. Contour lines at 1.1 km s^{-1} and 2.4 km s^{-1} represent estimates of the elevation of the base of saprolite and the base of weathered rock, respectively (Figure S3 in Supporting Information S1). The location of the line number in the inset map signifies the start of each line.

The depth to unoxidized bedrock ($V_P = 2.4$ km s^{-1}) ranges from 3 m near stream channels (e.g., Line 6 at 40 m) to 39 m at ridgetop positions (e.g., Line 1 at 50 m). In some cases the depth of investigation of the geophysical surveys is insufficient to capture the 2.4 km s^{-1} velocity boundary (e.g., Line 1 at 40 m).

3.3. Groundwater Levels in Deep Boreholes

At S3W1, the water table elevation varied between 755.7 and 756.7 m (25.2 and 24.3 m below the surface) from October 2022 to February 2023, and showed a gradual increase throughout the rainy winter months (Figure 4). At N4W1, the well was dry until late December. Following precipitation in December the water table elevation varied between 753.6 and 754.5 m (37.1 and 36.2 m below the surface) with the exception of three rapid increases in water level of ∼1–2 m in late December and early January, which was likely due to water flowing down the borehole during rainstorms. The in-stream well (StW1) shows water levels at elevations of 753.8–754.9 m (less than a meter below ground surface) with small fluctuations in November, followed by a gradual increase in early December before eventually reaching the ground surface elevation in mid-December and early-January.

4. Discussion

4.1. Drivers of Deep Subsurface Fracturing

The deep fracturing at Arbor Creek may be driven by the geologic history, the proximity to an active fault, or the regional stress regime. For example, the geology in the Diablo Range is characterized by the Franciscan Complex where sedimentary rocks have been deformed and metamorphosed before being exhumed during uplift of the California Coast Ranges (Blake & Wentworth, 1999). The lack of a coherent bedding plane (Figure S10 in Supporting Information S1) and the proximity of Arbor Creek to the geologic contact with mélange units with high-grade metamorphic minerals (Figure 1b) suggests that bedrock in the region experienced substantial reorganization, deformation, and fracturing during uplift of the California Coast Range (e.g., Page et al., 1998).

The close proximity of Arbor Creek to a creeping section of the Calaveras Fault may also cause significant fracturing (Figure 1a). The uplift of coherent blocks through fault zones causes deformation that is accommodated by significant fracturing (Molnar et al., 2007). Active tectonic processes can also cause fracturing due to the build up of inelastic strain generated during earthquakes and during interseismic periods (Cochran et al., 2009; Pollitz et al., 2004; Savage & Brodsky, 2011). Fault damage zones have typically been associated with areas directly adjacent to main faults. However, recent work has documented aftershocks and surface fracturing up to 20 km from main fault zones following major earthquakes (Rodriguez Padilla et al., 2022). Arbor Creek is only 2 km from the Calaveras fault, suggesting that uplift through faults and active tectonic processes may cause significant fracturing in underlying bedrock at Arbor Creek.

Subsurface fracturing has also been linked to subsurface stress fields due to the interaction of regional stresses with topography (Moon et al., 2020; St Clair et al., 2015). The modern tectonic environment in the California Coast Range is characterized by a series of transform faults. However, measurements of in situ stresses and modeling of uplift show a large component of fault-normal compression in the region (Montgomery, 1993; Zoback et al., 1987). The results from our seismic refraction surveys show large zones of low velocities beneath ridgetops, which is broadly consistent with weathering patterns at other sites with compressive regional stresses (St Clair et al., 2015). Given the complex geologic history and tectonic activity at Arbor Creek, the considerable fracturing is likely a result of several processes acting together, or at different magnitudes over geologic time.

More work is needed in geologically complex landscapes to tease apart the evolution of the critical zone, which can aid us in extrapolating these findings to other landscapes with similarly complex histories. The depth and degree of subsurface fracturing observed at Arbor Creek is greater than at Rancho Venada, a site in northern California with similar bedrock and climate that is located further from a major fault zone (Hudson Rasmussen et al., 2023; Pedrazas et al., 2021). This suggests that proximity to faults may play an important role in driving subsurface fracturing. However, more work examining how the extent of rock damage varies with distance from faults is needed to fully quantify the role of active tectonic processes in causing subsurface fracturing. Additionally, quantifying fracturing over greater depth would help constrain whether the fracturing is inherited before weathering occurs as proposed here, or controlled by patterns of meteoric water infiltration patterns which has been proposed in other systems (e.g., Ma et al., 2021). More work is also needed to evaluate the role of topographic stress in driving fracturing. Recent work in central Pennsylvania has suggested that fractures from topographic stresses may play a secondary role in controlling the depth of weathering in landscapes underlain by sedimentary rock (e.g., Ma et al., 2021; Wang et al., 2021). A direct comparison of seismic refraction surveys to models of topographic and regional stress would help constrain the role of modern stresses in controlling subsurface fracturing at Arbor Creek.

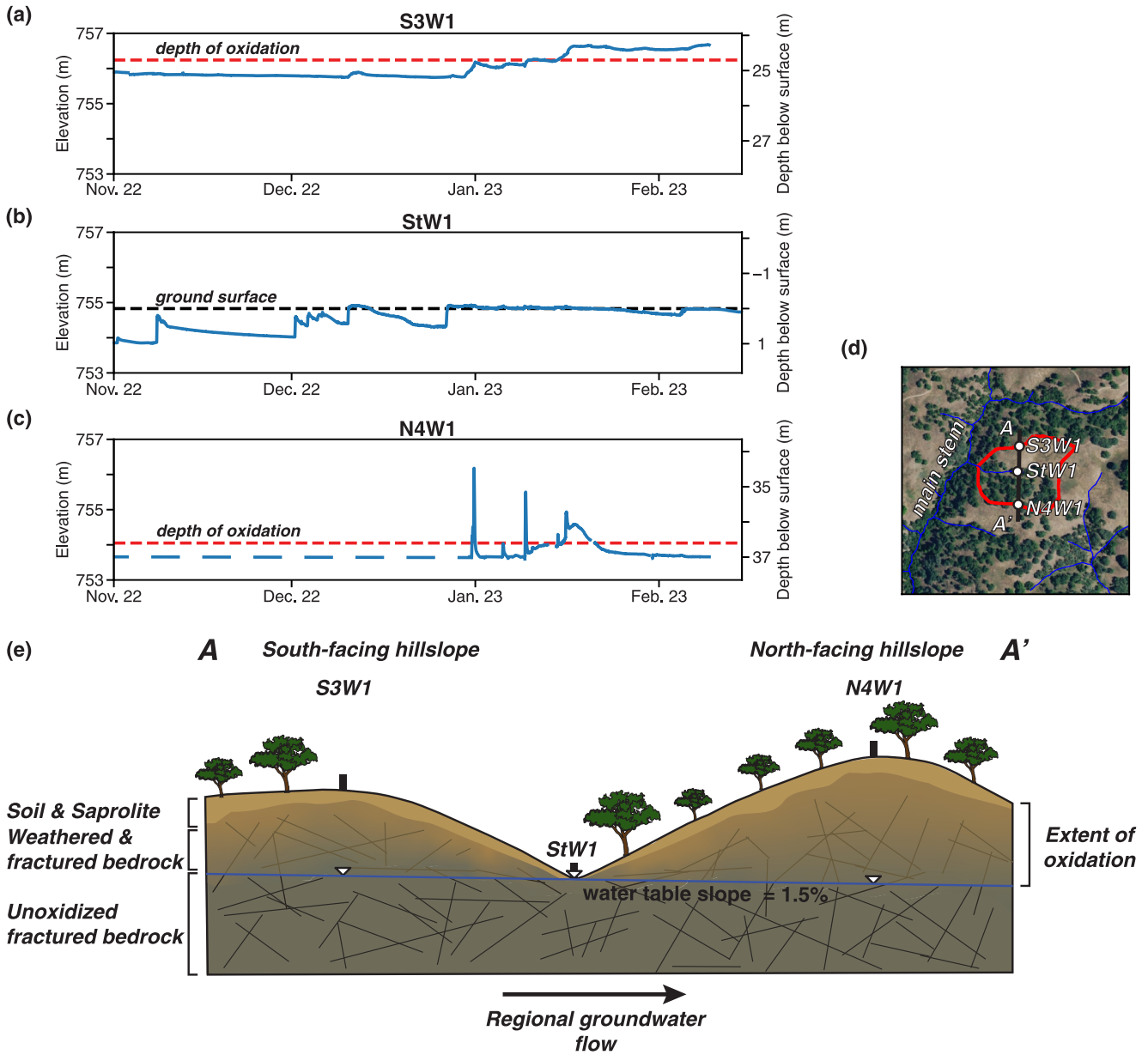

Figure 4. Groundwater levels and critical zone structure in Arbor Creek. Groundwater levels (blue lines) from November 2022 to February 2023 for S3W1 (a), StW1 (b), and N4W1 (c). The elevation of oxidation observed in the cores is shown as a dashed red line and the ground surface elevation at StW1 is shown as a dashed black line. Sharp increases in groundwater level at N4W1 are likely due to water running down the borehole during rain events. Dashed blue line represents dry conditions. The well locations and elevation transect from A to A' (d) was used to create a conceptual model (e) of interactions between fracturing, chemical weathering, and hydrologic processes based on field measurements. The core observations and geophysical data indicate a highly fractured subsurface that allows water to infiltrate deep into the subsurface causing oxidation of fractures (brown lines) down to the water table (blue line). The water infiltrating deep into the subsurface likely contributes to a regional groundwater system that flows at or just beneath the intermittent first-order stream channel.

4.2. Hydrologic Control on Chemical Weathering

The significant fracturing observed at Arbor Creek increases permeability and provides surface area for weathering reactions to take place, serving an important role in initiating weathering in the critical zone. However, in order for exposed surfaces to be chemically altered, oxygen-rich meteoric water must infiltrate and interact with mineral surfaces (e.g., Lebedeva & Brantley, 2013). The presence of oxidation along mineral surfaces can be used to understand subsurface flow paths of meteoric water. For example, in areas where oxidation is observed in the rock matrix and along fracture planes, meteoric water is likely flowing. In contrast, in the deeper sections of the

core where oxidation is restricted to fracture planes, the predominant flow paths of oxygen-rich meteoric water are likely fracture planes. Furthermore, in areas with no signs of oxidation, the water flowing along fracture planes is likely low in oxygen, saturated in weathering products, and unable to weather mineral surfaces. There are no signs of oxidation along fracture planes below 36.6 m at N4W1 and below 24.7 m at S3W1. These depths are roughly coincident with the observed depth of the water table at N4W1 and S3W1 (Figures 4a and 4c). The lack of weathering below the water table is consistent with previous work in sedimentary systems that has proposed that chemical weathering is initiated by the drainage of chemically equilibrated water and subsequent infiltration of oxygen-rich water into pore space and fractures (Rempe & Dietrich, 2014). While our observations are consistent with oxidation being limited by the water table depth, more work is needed to understand if hydrolysis reactions below the water table contribute to subsurface weathering (e.g., Ollier, 1988; Taylor & Eggleton, 2001). Additionally, more work is needed to understand if the relationship between the water table and the weathering front changes with topographic positions as observed in recent field (Gu et al., 2020; Sullivan et al., 2016) and modeling studies (Lebedeva & Brantley, 2020).

4.3. Implications for Critical Zone Hydrology

Together the observations of fracturing, oxidation, and groundwater levels suggest that fracturing enhances permeability driving cycling of meteoric water deep beneath the surface, which has important implications for groundwater recharge, streamflow generation, and interbasin water transfer. Since Arbor Creek is an intermittent first-order basin with limited upgradient groundwater sources, the deep groundwater observed here is likely maintained by recharge from local precipitation. The elevation of the water table was observed to be at or below the stream channel and is on average 2 m lower at N4W1 than at S3W1, leading to a water table slope that is ∼1.5%. This downslope gradient is roughly parallel to the mainstem of the watershed that our study system is nested within (Figure 4). Together, these observations suggest that water may be contributing to interbasin water transfer, or may be exiting the catchment in the subsurface, which is consistent with modeling efforts that predict large amounts of regional groundwater flow in high-relief landscapes with low ratios of recharge to hydraulic conductivity (Gleeson & Manning, 2008). This deep water movement likely recharges a regional groundwater system and has important implications for understanding streamflow generation (Montgomery et al., 1997; Oda et al., 2013) and regional groundwater supplies in higher order catchments (Fan, 2019; Shaman et al., 2004). Furthermore, this highlights the need to understand the weathering structure of the deep critical zone when considering deep hydrologic flow paths in headwater systems (Condon et al., 2020).

5. Conclusions

Measurements of subsurface weathering from borehole drilling and seismic refraction surveys show a highly fractured subsurface with oxidation 25–37 m below the ground surface in the study hillslopes of Arbor Creek. The significant and deep subsurface fracturing is likely due to a combination of factors, including rock deformation during uplift, fracturing from active tectonic processes on the nearby Calaveras Fault, and compressional regional stresses that may be compounded due to local conditions proximal to the active fault zone. The highly fractured bedrock facilitates water movement along deep flow paths, potentially contributing to the regional groundwater system and facilitating interbasin transfer of water. Additionally, the depth of oxidation is at similar depths to the water table, suggesting that chemical weathering is controlled by drainage of equilibrated water as rock is exhumed above the water table. Together this work yields new insights on the interplay between hydrologic flow paths and subsurface weathering in areas where geologic and tectonic processes cause deep and extensive fracturing in the subsurface. This work highlights the need for more measurements of subsurface weathering and hillslope hydrology in complex geologic and tectonic environments that drive significant fracturing of underlying bedrock.

Data Availability Statement

Geophysical data, groundwater data, and core images are available on Hydroshare (Callahan, 2024). Seismic refraction inversion code is archived on Zenodo (Huang, 2021). InSAR data was processed using the ISCE processing software (Rosen et al., 2018). UAVSAR images are available via the JPL UAVSAR Data Search (https://uavsar.jpl.nasa.gov/cgi-bin/data.pl).

Acknowledgments
This work was supported by NSF EAR CAREER Grant 2046957 to Margaret Zimmer. We thank Nerissa Barling, Bill Dietrich, David Dralle, Lauren Giggy, Jesse Hahm, Daniella Rempe, Daphne Smith, and Michael Wilshire for help during drilling. We thank Zac Harlow and Zac Tuthill for land access.

References

Andrews, E., & Navarre-Sitchler, A. (2021). Temporal and spatial heterogeneity of mineral dissolution rates in fractured media. *Geochimica et Cosmochimica Acta*, *312*, 124–138. https://doi.org/10.1016/j.gca.2021.08.008

Blake, M. C., & Wentworth, C. M. (1999). Structure and metamorphism of the Franciscan Complex, Mt. Hamilton area, northern California. *International Geology Review*, *41*(5), 417–424. https://doi.org/10.1080/00206819909465150

Brooks, B. A., Minson, S. E., Glennie, C. L., Nevitt, J. M., Dawson, T., Rubin, R., et al. (2017). Buried shallow fault slip from the South Napa earthquake revealed by near-field geodesy. *Science Advances*, *3*(7), e1700525. https://doi.org/10.1126/sciadv.1700525

Callahan, R. (2024). Supplement for "Geologic and tectonic controls on deep fracturing, weathering, and water flow in the central California Coast Range" [Dataset]. *Hydroshare*. https://doi.org/10.4211/hs.98a6cb4e3f0b49d2b6910c26a2d8f7f8

Callahan, R. P., Riebe, C. S., Pasquet, S., Ferrier, K. L., Grana, D., Sklar, L. S., et al. (2020). Subsurface weathering revealed in hillslope-integrated porosity distributions. *Geophysical Research Letters*, *47*(15), e2020GL088322. https://doi.org/10.1029/2020gl088322

Callahan, R. P., Riebe, C. S., Sklar, L. S., Pasquet, S., Ferrier, K. L., Hahm, W. J., et al. (2022). Forest vulnerability to drought controlled by bedrock composition. *Nature Geoscience*, *15*(9), 714–719. https://doi.org/10.1038/s41561-022-01012-2

Charles, J., & William, B. (2010). Fault activity map of California. https://maps.conservation.ca.gov/cgs/metadata/GDM_006_FAM_750k_v2_metadata.html#Distribution_Information

Cochran, E. S., Li, Y.-G., Shearer, P. M., Barbot, S., Fialko, Y., & Vidale, J. E. (2009). Seismic and geodetic evidence for extensive, long-lived fault damage zones. *Geology*, *37*(4), 315–318. https://doi.org/10.1130/G25306A.1

Condon, L. E., Markovich, K. H., Kelleher, C. A., McDonnell, J. J., Ferguson, G., & McIntosh, J. C. (2020). Where is the bottom of a watershed? *Water Resources Research*, *56*(3), e2019WR026010. https://doi.org/10.1029/2019wr026010

Dibblee, T. W., Jr., & Minch, J. A. (2005). *Geologic map of the Diablo quad-rangle, contra costa and alameda counties*. Dibblee Geo-logical Foundation (Santa Barbara Museum of Natural History). Dibblee Foundation Map DF-162, scale 1:24,000.

DiBiase, R. A., Rossi, M. W., & Neely, A. B. (2018). Fracture density and grain size controls on the relief structure of bedrock landscapes. *Geology*, *46*(5), 399–402. https://doi.org/10.1130/g40006.1

Donaldson, A., Dralle, D., Barling, N., Callahan, R. P., Loik, M. E., & Zimmer, M. (2024). Aspect Differences in Vegetation Type Drive Higher Evapotranspiration on a Pole-Facing Slope in a California Oak Savanna. *Journal of Geophysical Research: Biogeosciences*, *129*(7). https://doi.org/10.1029/2024jg008054

Donaldson, A. M., Zimmer, M., Huang, M.-H., Johnson, K. N., Hudson-Rasmussen, B., Finnegan, N., et al. (2023). Symmetry in hillslope steepness and saprolite thickness between hillslopes with opposing aspects. *Journal of Geophysical Research: Earth Surface*, *128*(7), e2023JF007076. https://doi.org/10.1029/2023jf007076

Dralle, D. N., Rossi, G., Georgakakos, P., Hahm, W. J., Rempe, D. M., Blanchard, M., et al. (2023). The salmonid and the subsurface: Hillslope storage capacity determines the quality and distribution of fish habitat. *Ecosphere*, *14*(2), e4436. https://doi.org/10.1002/ecs2.4436

Fan, Y. (2019). Are catchments leaky? *WIREs. Water*, *6*(6), e1386. https://doi.org/10.1002/wat2.1386

Fan, Y., Clark, M., Lawrence, D. M., Swenson, S., Band, L. E., Brantley, S. L., et al. (2019). Hillslope hydrology in global change research and earth system modeling. *Water Resources Research*, *55*(2), 1737–1772. https://doi.org/10.1029/2018wr023903

Flinchum, B. A., Holbrook, W. S., Grana, D., Parsekian, A. D., Carr, B. J., Hayes, J. L., & Jiao, J. (2018). Estimating the water holding capacity of the critical zone using near-surface geophysics. *Hydrological Processes*, *32*(22), 3308–3326. https://doi.org/10.1002/hyp.13260

Freeze, R., & Cherry, J. A. (1979). *Groundwater*. Prentice-Hall.

Gleeson, T., & Manning, A. (2008). Regional groundwater flow in mountainous terrain: Three-dimensional simulations of topographic and hydrogeologic controls. *Water Resources Research*, *44*(10), W10403. https://doi.org/10.1029/2008WR006848

Gu, X., Mavko, G., Ma, L., Oakley, D., Accardo, N., Carr, B. J., et al. (2020). Seismic refraction tracks porosity generation and possible CO2 production at depth under a headwater catchment. *Proceedings of the National Academy of Sciences of the United States of America*, *117*(32), 18991–18997. https://doi.org/10.1073/pnas.2003451117

Huang, M.-H. (2021). MongHanHuang/THB_rjMCMC: THB2D rjMCMC (V1.0.0.) [Software]. *Zenodo*. https://doi.org/10.5281/zenodo.4590999

Huang, M.-H., Hudson-Rasmussen, B., Burdick, S., Lekic, V., Nelson, M. D., Fauria, K. E., & Schmerr, N. (2021). Bayesian seismic refraction inversion for critical zone science and near-surface applications. *Geochemistry, Geophysics, Geosystems*, *22*(5), e2020GC009172. https://doi.org/10.1029/2020gc009172

Hubbert, M. K. (1940). The theory of ground-water motion. *The Journal of Geology*, *48*(8), 785–944. https://doi.org/10.1086/624930

Hudson Rasmussen, B. M., Huang, M.-H., Hahm, W. J., Rempe, D. M., Dralle, D., & Nelson, M. D. (2023). Mapping variations in bedrock weathering with slope aspect under a sedimentary Ridge-Valley system using near-surface geophysics and drilling. *Journal of Geophysical Research: Earth Surface*, *128*(7), e2023JF007254. https://doi.org/10.1029/2023jf007254

Krone, L. V., Hampl, F. J., Schwerdhelm, C., Bryce, C., Ganzert, L., Kitte, A., et al. (2021). Deep weathering in the semi-arid Coastal Cordillera, Chile. *Scientific Reports*, *11*(1). https://doi.org/10.1038/s41598-021-90267-7

Lebedeva, M. I., & Brantley, S. L. (2013). Exploring geochemical controls on weathering and erosion of convex hillslopes: Beyond the empirical regolith production function. *Earth Surface Processes and Landforms*, *38*(15), 1793–1807. https://doi.org/10.1002/esp.3424

Lebedeva, M. I., & Brantley, S. L. (2020). Relating the depth of the water table to the depth of weathering. *Earth Surface Processes and Landforms*, *45*(9), 2167–2178. https://doi.org/10.1002/esp.4873

Ma, L., Oakley, D., Nyblade, A., Moon, S., Accardo, N., Wang, W., et al. (2021). Seismic imaging of a shale landscape under compression shows limited influence of topography-induced fracturing. *Geophysical Research Letters*, *48*(17), e2021GL093372. https://doi.org/10.1029/2021gl093372

Mavko, G., Mukerji, T., & Dvorkin, J. (2009). *The rock physics handbook: Tools for seismic analysis of porous media*. Cambridge University Press.

McCormick, E. L., Dralle, D. N., Hahm, W. J., Tune, A. K., Schmidt, L. M., Chadwick, K. D., & Rempe, D. M. (2021). Widespread woody plant use of water stored in bedrock. *Nature*, *597*(7875), 225–229. https://doi.org/10.1038/s41586-021-03761-3

McIntosh, J. C., Schaumberg, C., Perdrial, J., Harpold, A., Vázquez-Ortega, A., Rasmussen, C., et al. (2017). Geochemical evolution of the Critical Zone across variable time scales informs concentration-discharge relationships: Jemez River Basin Critical Zone Observatory. *Water Resources*, *53*(5), 4169–4196. https://doi.org/10.1002/2016WR019712

Molnar, P., Anderson, R. S., & Anderson, S. P. (2007). Tectonics, fracturing of rock, and erosion. *Journal of Geophysical Research*, *112*(F3), F03014. https://doi.org/10.1029/2005jf000433

Montgomery, D. R. (1993). Compressional uplift in the central California Coast Ranges. *Geology*, *21*(6), 543. https://doi.org/10.1130/0091-7613(1993)021<0543:cuitcc>2.3.co;2

Montgomery, D. R., Dietrich, W. E., Torres, R., Anderson, S. P., Heffner, J. T., & Loague, K. (1997). Hydrologic response of a steep, unchanneled valley to natural and applied rainfall. *Water Resources Research*, *33*(1), 91–109. https://doi.org/10.1029/96WR02985

Moon, S., Perron, J. T., Martel, S. J., Goodfellow, B. W., Mas Ivars, D., Hall, A., et al. (2020). Present-day stress field influences bedrock fracture openness deep into the subsurface. *Geophysical Research Letters*, *47*(23), e2020GL090581. https://doi.org/10.1029/2020GL090581

Oda, T., Suzuki, M., Egusa, T., & Uchiyama, Y. (2013). Effect of bedrock flow on catchment rainfall-runoff characteristics and the water balance in forested catchments in Tanzawa Mountains, Japan. *Hydrological Processes*, *27*(26), 3864–3872. https://doi.org/10.1002/hyp.9497

Ollier, C. D. (1988). Deep weathering, groundwater and climate. *Geografiska Annaler—Series A: Physical Geography*, *70*(4), 285–290. https://doi.org/10.2307/521260

Page, B. M., Coleman, R. G., & Thompson, G. A. (1998). Late Cenozoic tectonics of the central and southern Coast Ranges of California. *GSA Bulletin*, *110*(7), 846–876. https://doi.org/10.1130/0016-7606(1998)110<0846:OLCTOT>2.3.CO;2

Payn, R. A., Gooseff, M. N., McGlynn, B. L., Bencala, K. E., & Wondzell, S. M. (2012). Exploring changes in the spatial distribution of stream baseflow generation during a seasonal recession. *Water Resources Research*, *48*(4), W04519. https://doi.org/10.1029/2011wr011552

Pedrazas, M. A., Hahm, W. J., Huang, M.-H., Dralle, D., Nelson, M. D., Breunig, R. E., et al. (2021). The relationship between topography, bedrock weathering, and water storage across a sequence of ridges and valleys. *Journal of Geophysical Research: Earth Surface*, *126*(4), e2020JF005848. https://doi.org/10.1029/2020jf005848

Pollitz, F., Bakun, W. H., & Nyst, M. (2004). A physical model for strain accumulation in the San Francisco Bay region: Stress evolution since 1838. *Journal of Geophysical Research*, *109*(B11), B11408. https://doi.org/10.1029/2004jb003003

Rempe, D. M., & Dietrich, W. E. (2014). A bottom-up control on fresh-bedrock topography under landscapes. *Proceedings of the National Academy of Sciences of the United States of America*, *111*(18), 6576–6581. https://doi.org/10.1073/pnas.1404763111

Rempe, D. M., & Dietrich, W. E. (2018). Direct observations of rock moisture, a hidden component of the hydrologic cycle. *Proceedings of the National Academy of Sciences of the United States of America*, *115*(11), 2664–2669. https://doi.org/10.1073/pnas.1800141115

Riebe, C. S., Hahm, W. J., & Brantley, S. L. (2017). Controls on deep critical zone architecture: A historical review and four testable hypotheses: Four testable hypotheses about the deep critical zone. *Earth Surface Processes and Landforms*, *42*(1), 128–156. https://doi.org/10.1002/esp.4052

Rodriguez Padilla, A. M., Oskin, M. E., Milliner, C. W. D., & Plesch, A. (2022). Accrual of widespread rock damage from the 2019 Ridgecrest earthquakes. *Nature Geoscience*, *15*(3), 222–226. https://doi.org/10.1038/s41561-021-00888-w

Rosen, P. A., Gurrola, E. M., Agram, P., Cohen, J., Lavalle, M., Riel, B. V., et al. (2018). The InSAR scientific computing environment 3.0: A flexible framework for NISAR operational and user-led science processing [Software]. In *IGARSS 2018—2018 IEEE International Geoscience and Remote Sensing Symposium* (pp. 4897–4900). IEEE. https://doi.org/10.1109/IGARSS.2018.8517504

Ruxton, B. P. V., & Berry, L. (1959). The basal rock surface on weathered granitic rocks. *Proceedings of the Geologists' Association. Geologists' Association*, *70*(4), 285–290. https://doi.org/10.1016/S0016-7878(59)80010-9

Savage, H. M., & Brodsky, E. E. (2011). Collateral damage: Evolution with displacement of fracture distribution and secondary fault strands in fault damage zones. *Journal of Geophysical Research*, *116*(B3), B03405. https://doi.org/10.1029/2010jb007665

Shaman, J., Stieglitz, M., & Burns, D. (2004). Are big basins just the sum of small catchments? *Hydrological Processes*, *18*(16), 3195–3206. https://doi.org/10.1002/hyp.5739

St Clair, J., Moon, S., Holbrook, W. S., Perron, J. T., Riebe, C. S., Martel, S. J., et al. (2015). Geophysical imaging reveals topographic stress control of bedrock weathering. *Science*, *350*(6260), 534–538. https://doi.org/10.1126/science.aab2210

Sullivan, P. L., Hynek, S. A., Gu, X., Singha, K., White, T., West, N., et al. (2016). Oxidative dissolution under the channel leads geomorphological evolution at the Shale Hills catchment. *American Journal of Science*, *316*(10), 981–1026. https://doi.org/10.2475/10.2016.02

Taylor, G., & Eggleton, R. A. (2001). *Regolith geology and geomorphology*. John Wiley and Sons.

Toth, J. (1963). A theoretical analysis of groundwater flow in small drainage basins. *Journal of Geophysical Research*, *68*(16), 4795–4812. https://doi.org/10.1029/JZ068i016p04795

Uchida, T., Asano, Y., Ohte, N., & Mizuyama, T. (2003). Seepage area and rate of bedrock groundwater discharge at a granitic unchanneled hillslope. *Water Resources Research*, *39*(1), 1018. https://doi.org/10.1029/2002wr001298

USGS. (2022). M 5.1—15km ESE of Alum Rock, CA. Retrieved February, 16 2024, from https://earthquake.usgs.gov/earthquakes/eventpage/nc73799091/executive

Wang, W., Nyblade, A., Mount, G., Moon, S., Chen, P., Accardo, N., et al. (2021). 3D seismic anatomy of a watershed reveals climate-topography coupling that drives water flowpaths and bedrock weathering. *Journal of Geophysical Research: Earth Surface*, *126*(12), e2021JF006281. https://doi.org/10.1029/2021jf006281

Zoback, M. D., Zoback, M. L., Mount, V. S., Suppe, J., Eaton, J. P., Healy, J. H., et al. (1987). New evidence on the state of stress of the San Andreas fault system. *Science*, *238*(4830), 1105–1111. https://doi.org/10.1126/science.238.4830.1105

References From the Supporting Information

Eppinger, B. J., Hayes, J. L., Carr, B. J., Moon, S., Cosans, C. L., Holbrook, W. S., et al. (2021). Quantifying depth-dependent seismic anisotropy in the critical zone enhanced by weathering of a Piedmont schist. *Journal of Geophysical Research: Earth Surface*, *126*(10), e2021JF006289. https://doi.org/10.1029/2021jf006289

Flinchum, B. A., Holbrook, W. S., & Carr, B. J. (2022). What do P-wave velocities tell us about the critical zone? *Frontiers in Water*, *3*, 772185. Retrieved from https://doi.org/10.3389/frwa.2021.772185

Novitsky, C. G., Holbrook, W. S., Carr, B. J., Pasquet, S., Okaya, D., & Flinchum, B. A. (2018). Mapping inherited fractures in the critical zone using seismic anisotropy from circular surveys. *Geophysical Research Letters*, *45*(7), 3126–3135. https://doi.org/10.1002/2017gl075976